33rd Annual International Conference of the IEEE EMBS
Boston, Massachusetts USA, August 30 - September 3, 2011

Orthogonal CSPAMM (OCSPAMM) MR Tagging for Imaging Ventricular Wall Motion

Hui Wang, Mo Kadbi, Melanie Kotys, Mehmet Ersoy, George P. Chatzimavroudis, Randolph M. Setser, Motaz Alshaher, Stefan E. Fischer, and Amir A. Amini, IEEE Fellow

***Abstract*— Tagged magnetic resonance imaging (MRI) has the ability to directly and non-invasively alter tissue magnetization and produce tags on the deforming tissue [1], [2]. Since its development, the Spatial Modulation of Magnetization (SPAMM) [2] tagging pulse sequence has been widely available and is the most commonly used technique for producing sinusoidal tag patterns. However, SPAMM suffers from tag fading which occurs in the later phases of the cardiac cycle. Complementary SPAMM (CSPAMM) was introduced to solve this problem by acquiring and subtracting two SPAMM images [3]. The drawback of CSPAMM is that it results in doubling of the acquisition time. In this paper, we propose a novel pulse sequence, termed Orthogonal CSPAMM (OCSAPMM), which results in the same acquisition time as SPAMM for 2D deformation estimation while keeping the advantages of CSPAMM. Different from CSPAMM, in OCSPAMM the second tagging pulse orientation is rotated 90 degrees relative to the first one so that motion information can be obtained simultaneously in two directions. A cardiac motion phantom, which independently models cardiac wall thickening and rotation in the human heart was used to show the effectiveness of the proposed pulse sequence.**

I. INTRODUCTION

Globally, cardiovascular disease is the number one cause of death and is projected to remain so in the foreseeable future [4]. Heart disease, such as myocardial ischemia, may be identified and localized through analysis of the cardiac deformation. Magnetic resonance imaging (MRI) is a highly advanced and sophisticated imaging modality for cardiac motion assessment and quantitative analysis, capable of providing 3D analysis of global and regional cardiac function with great accuracy and reproducibility. In recent times, MRI tagging has seen increased applications and is becoming the gold standard for quantifying regional function. Numerous efforts have been devoted to cardiac motion recovery and deformation analysis algorithms from tagged MR image sequences, including B-spline models [5], [6], deformable models [7], [8], non-rigid registration [9], Harmonic Phase (HARP) [10], Sine Wave Modeling (SinMod) [11], and multilevel B-splines with phase information [12], [13], among others.

Myocardial tagging was first introduced by Zerhouni *et al.* [1] and Axel *et al.* [2] in 1988 and 1989, respectively. It uses spin tagging prepulses to produce noninvasive markers in the myocardial tissues. The main reason why tagged MRI can image motion is that when the local magnetization of a material point is altered, the material point maintains the altered magnetization when it moves within the limits of the T_1 relaxation time resulting in tag fading. The varying magnetization produces alternating light and dark pattern on the image. Although Spatial Modulation of Magnetization (SPAMM) [2] is the most commonly used technique for tagging, it suffers from tag fading in the later phases of the cardiac cycle due to T_1 relaxation. Complementary SPAMM (CSPAMM) was introduced by Fischer *et al.* in order to mitigate the tag fading problem [3]. Although highly effective, one disadvantage of CSPAMM as originally proposed is that it doubles the image acquisition time, since it acquires two SPAMM images that are $180°$ out of phase prior to subtracting them for estimation of deformations in one direction. For 2D deformation estimation, CSPAMM requires four acquisitions. The interested reader is referred to reference [14] for a thorough review about cardiac MRI tagging techniques.

In this paper, we propose a novel tagging pulse sequence, Orthogonal CSPAMM (OCSPAMM), which results in the tag lines to be persistent over the entire length of the cardiac cycle while halving the imaging time, when compared to CSPAMM. In comparison to CSPAMM, OCSPAMM eliminates the DC interference of the off-center peaks [3], but does not produce tag patterns in the same direction that are 180 degrees out of phase.

Hui Wang, Mo Kadbi, and Amir A. Amini are with the Department of Electrical and Computer Engineering, University of Louisville, Louisville, KY, 40292 hui.wang@louisville.edu

Melanie Kotys and Stefan Fischer are with Philips Medical Systems Inc., Cleveland, OH, 44143

Mehmet Ersoy, Randolph M. Setser, and George P. Chatzimavroudis are with Department of Chemical and Biomedical Engineering, Cleveland State University, Cleveland, OH 44115

Mehmet Ersoy and Randolph M. Setser are with Cleveland Clinic, Cleveland, OH 44195

Motaz Alshaher is an assistant professor of Medicine (Cardiology) and medical director of Cardiac Critical Care Unit, University of Louisville Hospital, Louisville, KY 40202

II. METHODS

A. Complementary SPAMM

CSPAMM is based on the subtraction of two images with complementary signed tagging modulation. The diagram for the CSPAMM pulse sequence is shown in Fig. 1. The tagging pulses in (a) and (b) are out of phase by $180°$. By subtracting them, CSPAMM reduces tagline intensity fading and consequently allows longer net tag persistence throughout the heart cycle.

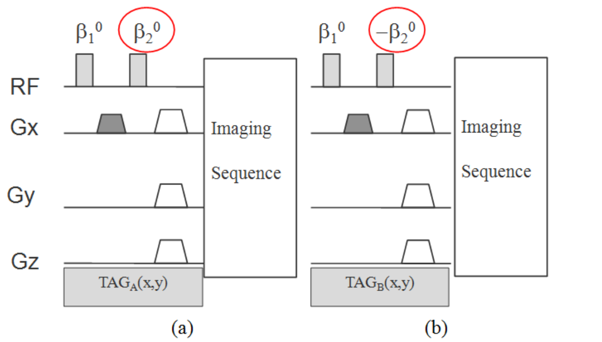

Fig. 1. Timing diagram of a 1-1 CSPAMM sequence. (a) Measurement with positive tagging pattern $TAG_A(x,y)$ (b) Measurement with negative tagging pattern $TAG_B(x,y)$

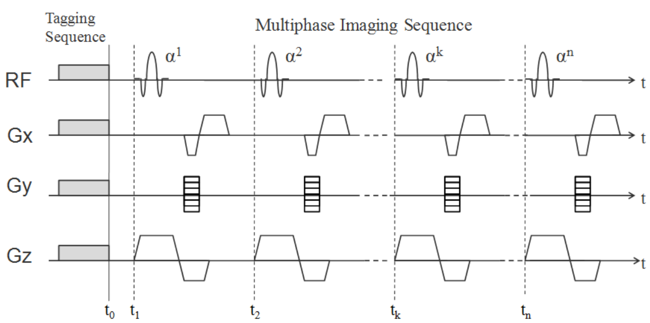

Fig. 2. Timing diagram of a typical tagging experiment. A tagging sequence is applied before t_0 followed by a standard multiphase imaging sequence. t_i corresponds to the start of the i^{th} phase in the cardiac cycle.

In CSPAMM, the longitudinal magnetization M_z is decomposed into two terms: one for tagging information Q_T, the other for the relaxation part Q_R. A timing diagram of a typical tagging experiment is shown in Fig. 2. At time t_0 right after the SPAMM tagging sequence, the modulated longitudinal magnetization is:

$$M_z(t_0) = M_{ss}TAG(x,y) \tag{1}$$

where M_{ss} is the steady state magnetization before tagging and $TAG(x,y)$ represents the spatial modulation of magnetization introduced by tagging sequence. At time t_1,

$$\begin{aligned} M_z(t_1) &= (M_z(t_0) - M_0)e^{-t_1/T_1} + M_0 \\ &= (M_{ss}TAG(x,y) - M_0)e^{-t_1/T_1} + M_0 \\ &= \underline{M_{ss}TAG(x,y))e^{-t_1/T_1}} + \underline{M_0(1 - e^{-t_1/T_1})} \\ &= Q_{T_1} + Q_{R_1} \end{aligned} \tag{2}$$

where M_0 is the equilibrium magnetization and T_1 is the longitudinal relaxation time. Recursively, at time t_k, two components of the longitudinal magnetization right before the k_{th} RF pulse are:

$$Q_{T_k} = M_{ss}TAG(x,y)e^{-t_k/T_1}\prod_{j=0}^{k-1}\cos\alpha_j \tag{3}$$

$$Q_{R_k} = (Q_{R_{k-1}}\cos\alpha_{k-1} - M_0)e^{-(t_k - t_{k-1})/T_1} + M_0 \tag{4}$$

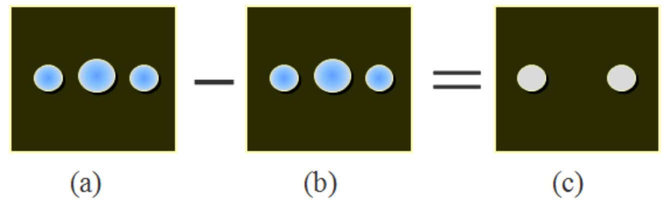

Fig. 3. Visualization of k-space for an image modulated by a cosine in the horizontal direction. (a)k-space for one SPAMM with positive tagging pattern (b)k-space for the other SPAMM with negative tagging pattern (c)k-space for CSPAMM

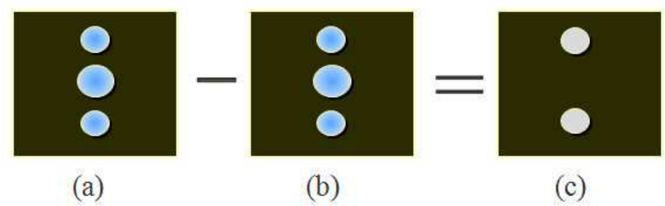

Fig. 4. Visualization of k-space for an image modulated by a cosine in the vertical direction. (a)k-space for one SPAMM with positive tagging pattern (b)k-space for the other SPAMM with negative tagging pattern (c)k-space for CSPAMM

where Q_{T_k} is the tagging component, while Q_{R_k} is the relaxed term. After the k_{th} RF imaging pulse of flip angle α_k, the longitudinal magnetization is rotated to the xy plane which contributes to the k_{th} image.

$$\begin{aligned} I_k &= M_z(t_k)\sin\alpha_k e^{-TE/T_2^*} \\ &= (Q_{T_k} + Q_{R_k})\sin\alpha_k e^{-TE/T_2^*} \end{aligned} \tag{5}$$

The basic idea of CSPAMM is to eliminate the relaxation term Q_{R_k} while only keeping the tagging information term Q_{T_k} by acquiring two images A_k and B_k using the same parameters except for their respective tagging patterns $TAG_A(x,y)$ and $TAG_B(x,y)$ (See Fig. 1). The subtraction of the k_{th} pair of images leads to

$$\begin{aligned} A_k - B_k &= M_{ss}[TAG_A(x,y) - TAG_B(x,y)] \\ &\quad \times e^{-t_k/T_1}(\prod_{j=0}^{k-1}\cos\alpha_j)\sin\alpha_k e^{-TE/T_2^*} \end{aligned} \tag{6}$$

Visualization of k-space for an image modulated by a cosine tagging function in the horizontal direction is shown in Fig. 3 and for the vertical direction is shown in Fig. 4. In both figures, (a) shows the k-space for the SPAMM with positive tagging pattern, (b) shows the k-space for the other SPAMM with negative tagging pattern, and (c) is the k-space for CSPAMM which is the subtraction of (b) from (a).

B. Orthogonal Complementary SPAMM (OCSPAMM)

As seen in Fig. 1, in CSPAMM, two SPAMM tagging sequences 180 degrees out of phase are placed in the same direction, either in frequency encoding or phase encoding direction, resulting in the need for 4 separate acquisitions.

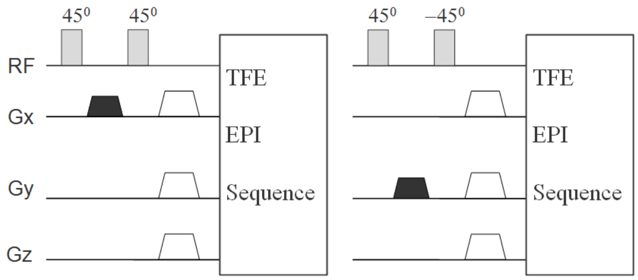

Fig. 5. Timing diagram for the OCSPAMM sequence. The first pair of 45° RF pulses with an interspersed tagging gradient are used to define the tags in G_x direction. The second pair of 45° RF pulses with an interspersed tagging gradient orthogonal to the first tagging gradient are used to define the tags in G_y direction. A TFE-EPI sequence is used for imaging as shown in Fig. 6.

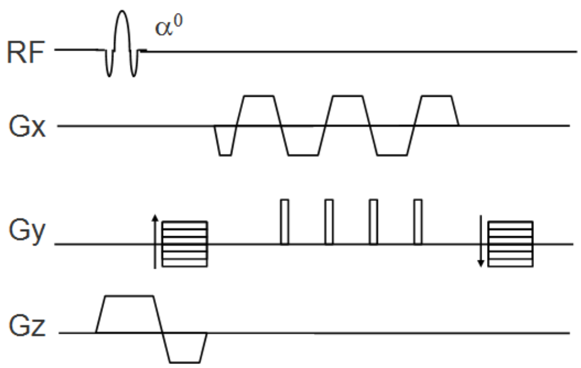

Fig. 6. A timing diagram of the TFE-EPI sequence used for imaging the modulated magnetization with EPI factor 5. After each RF pulse, five k-space profiles are acquired with the help of the blip gradients in phase encoding direction.

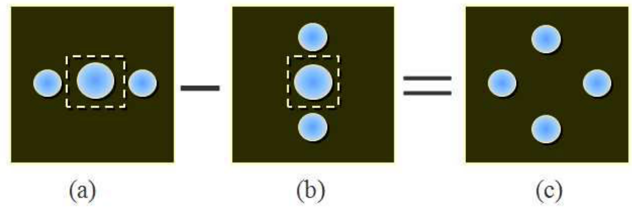

Fig. 7. Visualization of k-space for the OCSPAMM sequence. (a) k-space for tagged image with positive tagging pattern (b) k-space for tagged image with negative tagging pattern in orthogonal direction to (a) (c) k-space for OCSPAMM

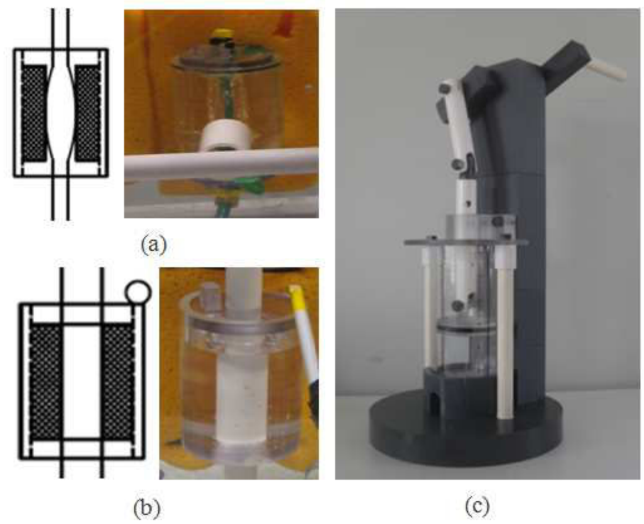

Fig. 8. Phantom components. (a) Contracting cardiac phantom (b) Rotating cardiac phantom (c) Air pump

In the proposed OCSPAMM sequence, the second SPAMM tag orientation is rotated 90 degrees relative to the first so that tag lines in two directions are combined (through subtraction) after only 2 acquisitions, therefore achieving removing of the central DC peak in k-space. The OCSPAMM sequence timing diagram is shown in Fig. 5. As it may be seen in this figure, the first tagging gradient is in the G_x direction, while the second tagging gradient is in the G_y direction. A TFE-EPI sequence is used to image the modulated magnetization, as shown in Fig. 6.

Visualization of k-space for OCSPAMM sequence is shown in Fig. 7. Similar to the CSPAMM sequence of Fig. 3, two SPAMM images are subtracted, but unlike the original CSPAMM technique, the second tagged acquisition is orthogonal to the first one. This approach eliminates the DC component while leaving the off-center peaks in k-space intact and reduces the acquisition time by a factor of two when compared to the original CSPAMM technique.

III. Results

A cardiac motion phantom, which independently models myocardial wall thickening and rotation in the human heart, was utilized to test the proposed OCSPAMM pulse sequence. The main elements of the LV motion phantom are the air pump, two phantoms within a common enclosure, trigger circuit, and rotation motion actuator. The two phantoms and the air pump are shown in Fig. 8. Other than the triggering circuit, all material used in construction of the phantom were non-ferromagnetic and MR compatible (polycarbonate, wood, latex, sponge, di-electric gel) [15].

All imaging experiments were conducted on a 3T Achieva MR scanner (Philips Healthcare, Best, NL) using a two element receive coil. The tag line distance was 7 mm. The phantom was imaged using a turbo gradient echo-echo planar imaging cine pulse sequence (Fig. 6) with the following parameters: TR/TE = $9.1/4.7$ ms, $10°$ flip angle, turbo factor 7, FOV 225×225 mm, in-plane voxel size 2×2 mm^2, reconstruction resolution 1.25×1.25 mm^2, slice thickness 8 mm, 14 heart phases, 112×85 acquired matrix, EPI factor 5. The cardiac cycle was approximately 1000 ms and T_1 of dielectric gel in the phantom was 728 ms (similar to myocardial tissue, in-vivo).

Two experiments were conducted on the cardiac phantom to validate the proposed OCSPAMM tagging sequence: one for rotation as shown in Fig. 9 and the other for contraction as shown in Fig. 11. Seven images from fourteen cardiac phases are displayed. Every other frame during an entire cardiac cycle is chosen. The displaying order is from top-

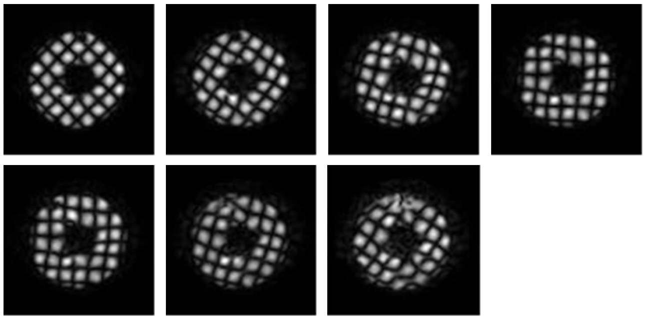

Fig. 9. Seven Images from fourteen cardiac phases for a rotating phantom using the proposed OCSPAMM pulse sequence. Every other frame during an entire cardiac cycle is shown. The order is from top-left to bottom-right.

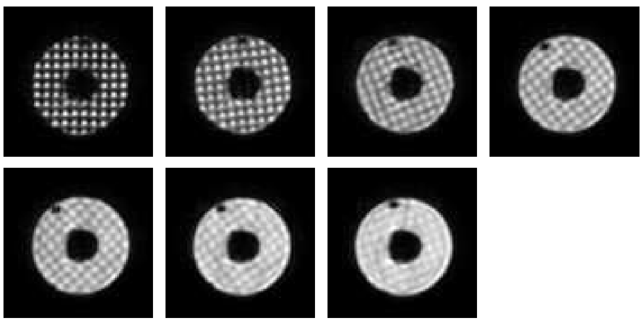

Fig. 10. Seven images of fourteen cardiac phases during an entire cardiac cycle for a rotating phantom using SPAMM pulse sequence. Every other frame is shown. The order is from top-left to bottom-right. In comparison to images acquired with OCSPAMM from the same phantom (Fig. 9), tag fading is clearly evident.

left to bottom-right. The OCSPAMM tagged images showed good image quality and persistent tag contrast for the entire duration of the cardiac cycle. For comparison to SPAMM sequence, Fig. 10 shows a cine sequence of SPAMM tagging on the same rotating phantom during one cardiac cycle, where tag fading is clearly evident. Notice that there are some artifacts in the upper and lower portion of the last frame in Fig. 11. These were due to susceptibility from the air inside the center of the phantom and are unrelated to the OCSPAMM pulse sequence.

IV. Conclusions

In this paper, we have proposed a novel tagging pulse sequence called OCSPAMM. OCSPAMM acquires tagged data in two orthogonal directions within the same time as the commonly used SPAMM acquisition procedure which acquires two data sets, each with a set of 1D linear tags orthogonal to one another. However, relative to SPAMM, OCSPAMM has the advantage of eliminating the DC peak which contributes significantly to the loss of tag-myocardium contrast (the term Q_{R_k} in equation 4.) We demonstrated the effectiveness of OCSPAMM on a dynamic cardiac phantom for both rotation and contraction. In-vivo imaging with OCSPAMM will be undertaken next.

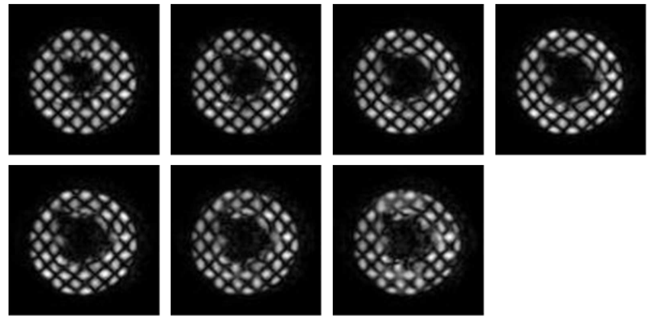

Fig. 11. Seven Images from fourteen cardiac phases for a contracting phantom using the proposed OCSPAMM pulse sequence. Every other frame during an entire cardiac cycle is shown. The order is from top-left to bottom-right.

References

[1] E. Zerhouni, D. Parish, W. Rogers, A. Yang, and E. Shapiro, "Human heart: Tagging with MR imaging–a method for noninvasive assessment of myocardial motion," *Radiology*, vol. 169, pp. 59–63, 1988.

[2] L. Axel and L. Dougherty, "MR imaging of motion with spatial modulation of magnetization," *Radiology*, vol. 171, pp. 841–845, 1989.

[3] S. E. Fischer, G. C. McKinnon, S. E. Maier, and P. Boesiger, "Improved myocardial tagging contrast," *Magnetic Resonance in Medicine*, vol. 30, no. 2, pp. 191–200, August 1993.

[4] World Health Organization, "Cardiovascular diseases," http://www.who.int/entity/nmh/publications/fact_sheet_cardiovascular_en.pdf.

[5] J. Huang, D. Abendschein, V. G. Dávila-Román, and A. A. Amini, "Spatio-temporal tracking of myocardial deformations with a 4-D B-spline model from tagged MRI," *IEEE Trans. Med. Imag.*, vol. 18, no. 10, pp. 957–972, October 1999.

[6] N. J. Tustison and A. A. Amini, "Biventricular myocardial strains via nonrigid registration of anatomical NURBS models," *IEEE Trans. Med. Imag.*, vol. 25, no. 1, pp. 94–112, January 2006.

[7] Z. Hu, D. Metaxas, and L. Axel, "In vivo strain and stress estimation of the heart left and right ventricles from MRI images," *Medical Image Analysis*, vol. 7, no. 4, pp. 435–444, December 2003.

[8] Ting Chen, Xiaoxu Wang, Sohae Chung, Dimitris Metaxas, and Leon Axel, "Automated 3D motion tracking using Gabor filter bank, robust point matching, and deformable models," *IEEE Trans. Med. Imag.*, vol. 29, no. 1, pp. 1–11, January 2010.

[9] R. Chandrashekara, R. H. Mohiaddin, and D. Rueckert, "Analysis of 3-D myocardial motion in tagged MR images using nonrigid image registration," *IEEE Trans. Med. Imag.*, vol. 23, no. 10, pp. 1245–1250, October 2004.

[10] N. F. Osman, E. R. McVeigh, and J. L. Prince, "Imaging heart motion using harmonic phase MRI," *IEEE Trans. Med. Imag.*, vol. 19, no. 3, pp. 186–202, March 2000.

[11] T. Arts, F. W. Prinzen, T. Delhaas, J. Milles, A. Rossi, and P. Clarysse, "Mapping displacement and deformation of the heart with local sine wave modeling," *IEEE Trans. Med. Imag.*, vol. 29, no. 5, pp. 1114–1123, May 2010.

[12] Hui Wang and A. A. Amini, "Accurate 2-D cardiac motion tracking using scattered data fitting incorporating phase information from MRI," in *Proceedings of SPIE Medical Imaging 2010: Biomedical Applications in Molecular, Structural, and Functional Imaging*, February 2010, vol. 7626.

[13] Hui Wang and A. A. Amini, "Cardiac motion tracking approach with multilevel B-splines and SinMod from tagged MRI," in *Proceedings of SPIE Medical Imaging 2011: Biomedical Applications in Molecular, Structural, and Functional Imaging*, February 2011, vol. 7965.

[14] V. M. Pai and L. Axel, "Advances in MRI tagging techniques for determining regional myocardial strain," *Current Cardiology Reports*, vol. 8, no. 1, pp. 53–58, 2006.

[15] M. Ersoy, M. Kotys, X. Zhou, and R. M. Setser, "A left ventricular motion phantom for cardiac MRI," in *Biomedical Engineering Society (BMES) 2010 Annual Meeting*, October 2010.